Nuclear Instruments and Methods in Physics Research B 330 (2014) 55–60

Contents lists available at ScienceDirect

Nuclear Instruments and Methods in Physics Research B

journal homepage: www.elsevier.com/locate/nimb

Microstructure evolution in Xe-irradiated UO_2 at room temperature

L.F. He [a,*], J. Pakarinen [a], M.A. Kirk [b], J. Gan [c], A.T. Nelson [d], X.-M. Bai [c], A. El-Azab [e], T.R. Allen [a,c]

[a] Department of Engineering Physics, University of Wisconsin-Madison, Madison, WI 53706, USA
[b] Argonne National Laboratory, Argonne, IL 60439, USA
[c] Idaho National Laboratory, Idaho Falls, ID 83415, USA
[d] Los Alamos National Laboratory, Los Alamos, NM 87545, USA
[e] School of Nuclear Engineering and School of Materials Engineering, Purdue University, West Lafayette, IN 47907, USA

ARTICLE INFO

Article history:
Received 24 January 2014
Received in revised form 12 March 2014
Accepted 12 March 2014
Available online 20 April 2014

Keywords:
Nuclear fuel
TEM
Irradiation
Dislocation
Inert gas bubble

ABSTRACT

In situ Transmission Electron Microscopy was conducted for single crystal UO_2 to understand the microstructure evolution during 300 keV Xe irradiation at room temperature. The dislocation microstructure evolution was shown to occur as nucleation and growth of dislocation loops at low irradiation doses, followed by transformation to extended dislocation segments and tangles at higher doses. Xe bubbles with dimensions of 1–2 nm were observed after room-temperature irradiation. Electron Energy Loss Spectroscopy indicated that UO_2 remained stoichiometric under room temperature Xe irradiation.

Published by Elsevier B.V.

1. Introduction

Fission gases such as Xenon (Xe) and Krypton (Kr) are among the most important fission products in UO_2 fuel. Because these elements are chemically inert, small traces of them tend to remain in the fuel matrix while the majority of these elements produced by the fission process tend to leave the fuel altogether and reside in the fuel plenum, or form fission gas bubbles. The control of these elements is important because of the associated radioactivity. The presence of these gases whether in matrix or in bubble form in the fuel leads to fuel property degradation [1]. While the behavior of fission gases in UO_2 fuel has been a focus of attention for a long time, there has been a recent surge in interest of modeling their release from fuel as part of a more comprehensive modeling of fuel microstructure and its impact on fuel properties [2,3]. An improved experimental understanding is required to support such a modeling effort. The present investigation, which aims to understand microstructure evolution in UO_2 under Xe ion irradiation, will ultimately support such a modeling effort as well as enable fundamental studies of thermal transport in Xe-containing UO_2.

Ion irradiation techniques have been widely used in the past decades to study the formation and evolution of defects and microstructure in UO_2. The formation of extended defects such as dislocations and cavities strongly depend on the temperature and ion fluence. Evans [4] found that a threshold implantation temperature at or above 500 °C was necessary for observing bubbles in Kr and Xe irradiated UO_2 by Transmission Electron Microscopy (TEM). He concluded that the threshold temperature for bubble nucleation is in the range of 350–500 °C. Sabathier et al. [5] studied the conditions for Xe precipitation into bubbles and found that the threshold temperature for Xe precipitation depended on the Xe fluence or concentration in polycrystalline UO_2. At a fluence of 2×10^{15} Xe/cm^2 (~0.4 at.%), the threshold temperature for bubble precipitation to occur was about 600 °C. At 1×10^{16} Xe/cm^2 (~2 at.%), however, this temperature was only about 400 °C. Sattonnay et al. [6] determined the bubble nucleation temperature of 400 °C in Xe-implanted single crystal UO_2 with a fluence of 8×10^{15} Xe/cm^2 by post-irradiation annealing. *In situ* observation from Michel et al. [7] showed the presence of subnanometer Xe bubbles in polycrystalline UO_2 irradiated to a low fluence (6×10^{12} Xe/cm^2) at 600 °C. All these previous studies show that both the temperature and ion dose play a key role in bubble nucleation and growth.

Another aspect of microstructure evolution in ion-irradiated UO_2 is the formation of extended defects such as dislocation loops and dislocation lines. *In situ* observations for dislocation evolution have been conducted for Xe- and Cs-irradiated polycrystalline UO_2 at room temperature as well as Kr-irradiated UO_2 single crystals at 600 and 800 °C [5,8]. The dislocation evolution in UO_2 is generally shown to occur by loop nucleation and growth mechanism at low

* Corresponding author. Tel.: +1 608 890 3579; fax: +1 608 263 7451.
E-mail address: lhe33@wisc.edu (L.F. He).

http://dx.doi.org/10.1016/j.nimb.2014.03.018
0168-583X/Published by Elsevier B.V.

irradiation doses, followed by transformation to extended dislocation segments and networks at high doses [8]. All these radiation-induced microstructural features affect the fuel performance, especially thermal transport properties. Therefore, investigating the production of point defects and the clustering of such defects into loops and gas bubbles is important. Particularly, investigation of the dynamic evolution process at different stages (by *in situ* observations) and their physical mechanisms is of great importance in understanding the degradation of physical properties of nuclear fuels.

In this work, *in situ* TEM has been used to study the dynamic evolution of dislocations in single crystal UO_2 irradiated with 300 keV Xe at room temperature. *Ex situ* TEM has also been used to investigate bubble evolution. Generally, the observed dislocation evolution is consistent with the results reported in literature for Xe- and Cs-irradiated polycrystalline UO_2 at room temperature [5] and with Kr-irradiated UO_2 single crystals at high temperatures [8]. The bubbles in UO_2 irradiated with Xe at room temperature are investigated here for the first time.

2. Experimental

Depleted UO_2 single crystal was fabricated at Chalk River Laboratories by heating fused UO_2 with hyperstoichiometric UO_2 to 1900 K in hydrogen. A lattice parameter a of 5.473 ± 0.001 Å was determined by neutron diffraction measurements at room temperature [9], which indicates that the stoichiometric ratio (O/U) is very close to 2.00 [10]. *In situ* irradiation thin foil specimens with a diameter of 3 mm were prepared by ultrasonic slicing, disc cutting and mechanical grinding to ~100 μm, dimpling down to ~20 μm at the center of the disc, and ion milling at 4.0 keV to perforation. The final polishing was performed with a 2 keV Ar ion beam. The orientation of the disc foils was close to <1 1 1> zone determined by electron diffraction pattern.

The *in situ* irradiation with ion beams was carried out with a Tandem implanter, coupled with a 300 kV Hitachi 9000 NAR TEM, at the Intermediate Voltage Electron Microscope (IVEM)-Tandem facility at the Argonne National Laboratory (ANL). The 30° incidence of the ion beam from the microscope optical axis, along with the integrated cameras, permits continuous observation and data recording during irradiation. Since the specimen was normally tilted about 15° facing the ion beam during irradiation, the actual angle between the ion beam and normal direction of specimen surface was about 15°. The 300 keV single-charged Xe ions were selected to produce the desired irradiation damage levels and depths. The single crystal UO_2 disc foil was irradiated at room temperature up to 1×10^{16} ions/cm^2.

A cross section perpendicular to as-irradiated TEM disc foil with 300 keV Xe up to 1×10^{16} ions/cm^2 was prepared by focused ion beam (FIB). The surface of irradiated foil at a thickness over 10 μm was coated by a platinum layer to protect the irradiated surface layer before ion milling. The FIB lamella was then characterized with a Tecnai TF30-FEG STwin TEM. Both Electron Dispersive X-ray Spectroscopy (EDS) and Electron Energy Loss Spectroscopy (EELS) in Scanning TEM (STEM) mode were employed to study the composition and microchemistry of the irradiated UO_2.

The Stopping and Range of Ions in Matter (SRIM) computer code [11] was used to simulate the profiles of atomic displacements in UO_2 as a function of depth. The threshold displacement energies for oxygen and uranium were set to 20 and 40 eV, respectively, which were determined by Soullard in his electron irradiation experiments in UO_2 [12]. The simulation was performed in the Kinchin-Pease damage calculation mode [13]. Fig. 1 shows the damage and Xe distribution profiles calculated by SRIM. The damage peak is at around a depth of 22 nm, increases from 3.4 dpa at a dose of 5×10^{14} ions/cm^2 to 68.7 dpa at a dose of 1×10^{16} ions/cm^2. The Xe concentration reaches a peak value at a depth of 54 nm. It increases from 0.1 at.% at a dose of 5×10^{14} ions/cm^2 to 1.9 at.% at a dose of 1×10^{16} ions/cm^2.

3. Results and discussion

Fig. 2 shows the *in situ* TEM images of the dislocation evolution in the UO_2 single crystal irradiated with 300 keV Xe ions at room temperature up to different dose levels. The bright field images (Fig. 2(a)–(d)) were shot at a diffraction condition of $g = 220$ and dark field images (Fig. 2(e)–(h)) were taken at a (g, $4g$), $g = 220$ weak-beam diffraction condition and the electron beam direction (B) was close to [1 1 1]. Some tiny defects could be detected in the sample before Xe irradiation (Fig. 2(a) and (e)), which are likely induced by the Ar ion-milling. As the Xe ion dose increased to 5×10^{14} ions/cm^2, high-density black dots appeared in the bright field image (Fig. 2(b)) and white dots in the dark field image (Fig. 2(f)). Similar features have also been found in UO_2 under fission damage [14,15] and in Kr and Xe ion irradiated UO_2 [5,8] and identified as small dislocation loops. The average size and density of dislocation loop at 5×10^{14} ions/cm^2 are 7.4 ± 3.1 nm and $(2.5 \pm 0.3) \times 10^{22}$ m^{-3}, respectively. The dislocation loops grew quickly with increasing the Xe ion fluence and interacted with each other at around 1×10^{15} ions/cm^2 (Fig. 2(c) and (g)), and finally transformed to dislocation tangles at higher doses (Fig. 2(d) and (h)). Due to high density of dislocations, it was difficult to quantitatively estimate loop density at the dose above 1×10^{15} ions/cm^2.

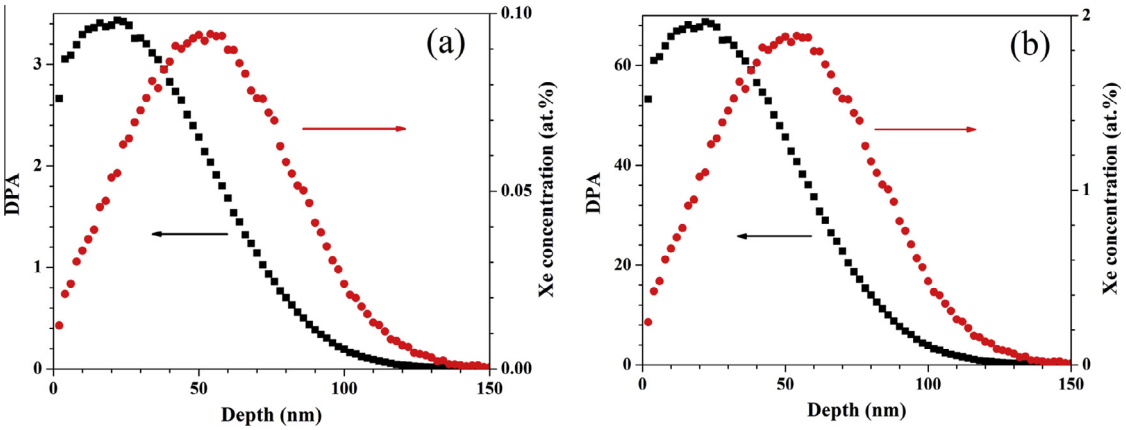

Fig. 1. Depth profiles of radiation damage and Xe concentration obtained from SRIM simulation of UO_2 subjected to Xe ion irradiation at room temperature with a total dose of (a) 5×10^{14} and (b) 1×10^{16} ions/cm^2.

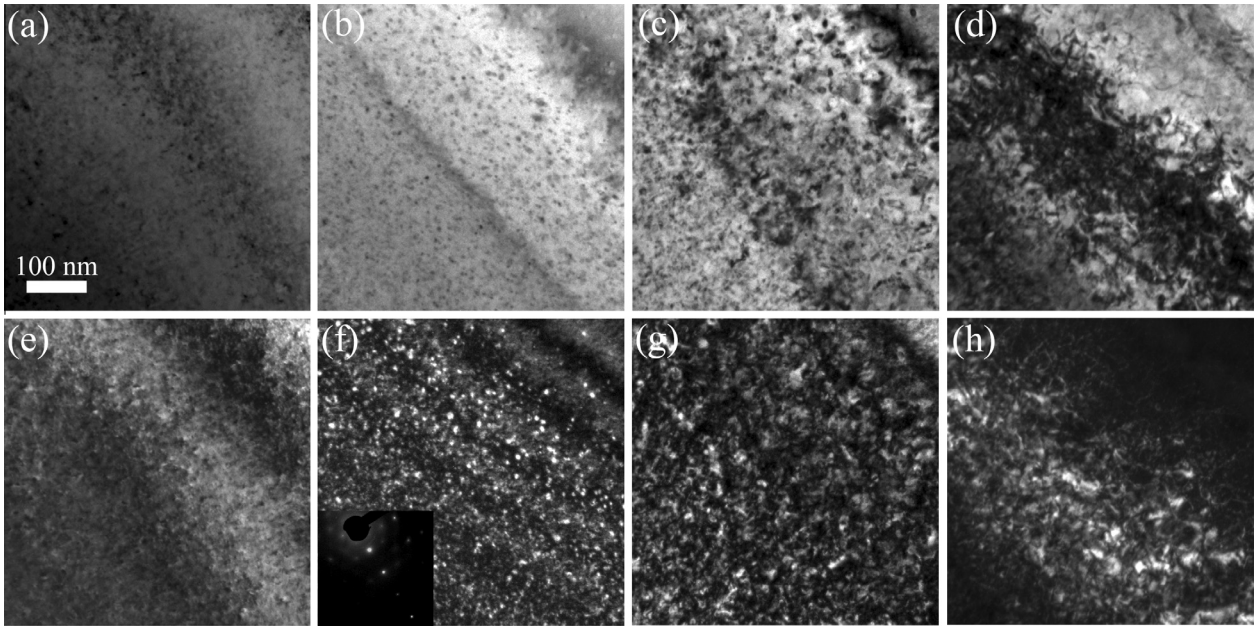

Fig. 2. Sequential bright field (BF) and dark field (DF) TEM images showing the nucleation and growth of defects in UO_2 single crystal irradiated with 300 keV Xe at room temperature at various dose levels: (a) and (e) no dose; (b) and (f) 5×10^{14} ions/cm^2; (c) and (g) 1×10^{15} ions/cm^2; (d) and (h) 1×10^{16} ions/cm^2. (a)–(d) are bright field images and (e)–(f) are dark field images. The observations were carried out from the [111] direction with g = 220 reflection for BF images and (g, 4g), g = 220 reflection for DF images. The inset in (f) shows the diffraction pattern.

The dislocation evolution (i.e., small loops → large loops → dislocation segments → dislocation tangle) with increasing irradiation dose at room temperature is similar to the trend observed in fission damaged UO_2 [14] as well as Xe, Cs, and Kr irradiated UO_2 under different irradiation energies [5,8]. At the highest dose of 1×10^{16} ions/cm^2, small isolated dislocation loops around 5 nm in diameter could still be found in the cross section TEM image (Fig. 3), indicating that new dislocation loops nucleate continuously as irradiation proceeds. In addition, the measured damage range of about 150 nm is in good agreement with theoretical calculations by SRIM (Fig. 3). However, there is no dislocation denuded zone near surface, which has been observed in 1 MeV Kr-irradiated UO_2 single crystal up to a dose of 5×10^{15} ions/cm^2 at 800 °C [8]. Generally, the denuded zones arise when the damage is created in the bulk or deep enough into the sample and defects are mobile. In the present case, the irradiation damage is very close to the surface, which caused dislocation nucleation to occur where the damage is, especially at low temperature. Further, at a lower irradiation temperature (room temperature compared with 800 °C), the mobility of point defects is much lower and thus less interstitials can escape to the surface. At a low irradiation temperature, some observed dislocation loops could nucleate directly from cascade damage and such a process does not require uranium interstitials to be mobile. Dislocation loop nucleation in UO_2 has been observed directly in simulation of cascade overlaps and it results from a loop punching process [16]. In previous Kr-irradiation experiments at 800 °C, thanks to higher mobility of uranium interstitials the loop growth becomes increasingly important for the formed microstructure. On the other hand, the average damage level at the first 20 nm depth in this study is about 5–6 times of that in Kr-irradiated UO_2. Higher point defects and extended defects should be produced in this work.

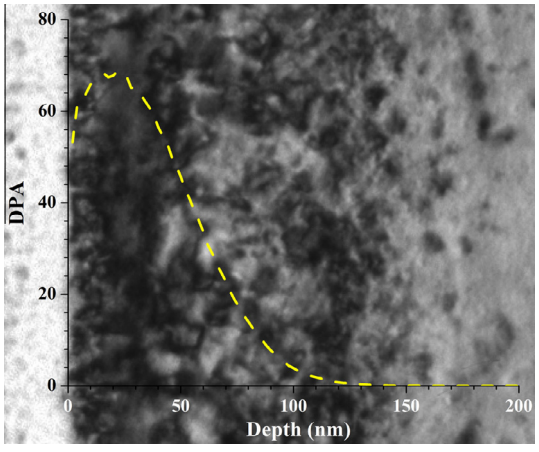

Fig. 3. Bright field TEM image showing the cross section of UO_2 single crystal irradiated with 300 keV Xe at room temperature at a dose of 1×10^{16} ions/cm^2. The plot shows the SRIM calculation of the damage profile.

Bright field images were taken at under-focus and over-focus conditions to confirm the presence of bubbles in the sample. Typically, small bubbles are seen as white and black dots at under and over-focus conditions, respectively. In both, 5×10^{14} and 1×10^{16} ion/cm^2 samples, small bubbles can be confirmed (Fig. 4(a)–(d)) and the average size of the bubbles was 1.9 ± 0.3 nm and 1.4 ± 0.2 nm, respectively and the bubble densities were $(1.4 \pm 0.3) \times 10^{24}$ and $(1.1 \pm 0.2) \times 10^{24}$ m^{-3}. Slight shrinkage of Xe bubbles has been reported in the dose range of 6×10^{13} and 2×10^{14} ions/cm^2 during *in situ* irradiation at 600 °C [7]. However, the detailed mechanisms for shrinkage have not been identified. The bubble density seems saturated in the dose range of 5×10^{14} to 1×10^{16} ion/cm^2, i.e. bubble density did not change with the dose level. Michel et al. [7] found that bubble density reached a saturation at a dose above 10^{14} ions/cm^2 in the *in situ* Xe irradiation of UO_2. However the mechanism of Xe re-solution or radiation induced bubble destruction is not convincing to explain this observation [7]. Therefore, no clear explanation can be given here for the saturation of bubble density and more work is needed. Note that the images of Fig. 4(a)–(d) were taken after irradiation and images are not from the same sample and same

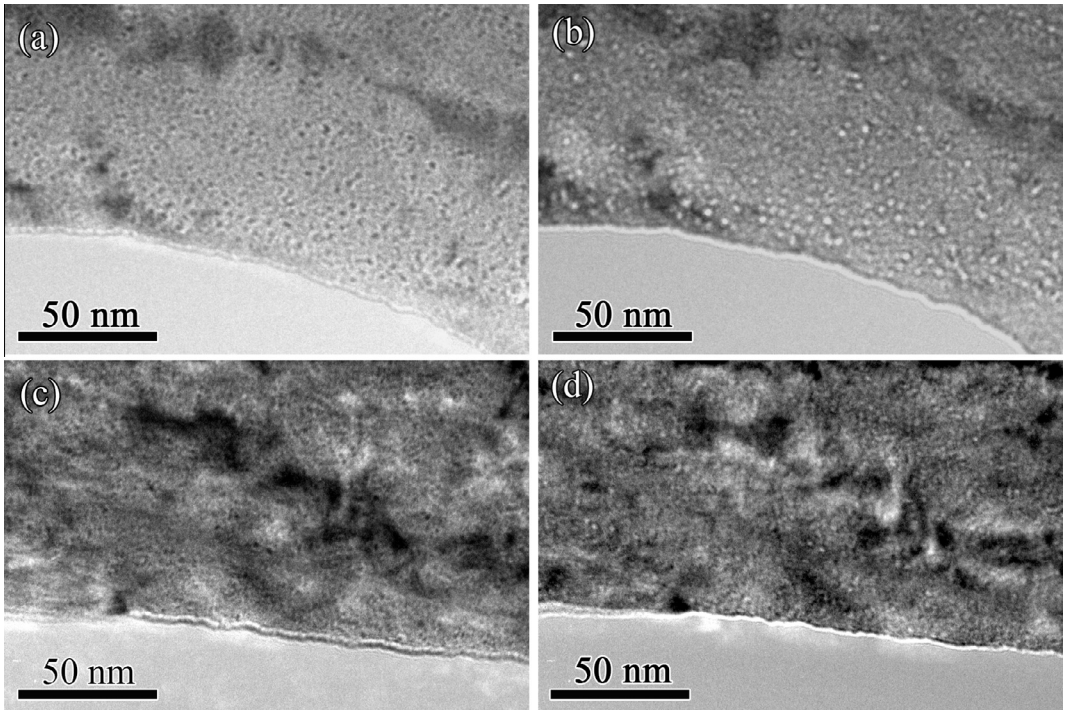

Fig. 4. TEM images of bubbles in Xe implanted UO_2 single crystal at a dose of 5×10^{14} (a and b) and 1×10^{16} ions/cm^2 (c and d). (a) And (c) are overfocus images and (b) and (c) are underfocus images.

position, so direct comparison of bubble size and density needs to be careful. To our knowledge, the nucleation of bubbles under ion irradiation at room temperature was confirmed by TEM observation for the first time. In the past studies, a threshold temperature above a few 100 °C is necessary [2–5]. The observation may indicate that some Xe bubbles may directly nucleate at the vacancy clusters produced in cascades and such a process does not require Xe and uranium vacancies to be diffusive. Fig. 5(a) shows the HRTEM image of Xe-implanted UO_2, which was taken from the [1 1 0] zone. Fig. 5(b) is the under-focus image of Fig. 5(a). The marked light-colored features in Fig. 5(a) match well with the white ones in Fig. 5(b), which corresponds to Xe bubbles. In addition, the lattice images show no significant differences in the bubble areas as compared to the UO_2 matrix, which indicates that there is no solid Xe precipitates associated with the bubbles. Solid precipitates in vicinity of the bubbles were reported by Nogita and Une in spent UO_2 fuel pellets with 45–83 GWd/ton [17,18]. They found Moiré fringes with the bubble areas in the HRTEM images and extra spots in the diffraction patterns. However, similar Moiré fringes were not found in the Kr bubbles in this work, confirming the lack of solid precipitates. The observation is in good agreement with the nature of Kr bubbles in CeO_2 [19].

Garrido et al. [20] proposed two contributions responsible for the increase of the accumulated disorder: (i) displacement of lattice atoms by irradiation (ballistic contribution); (ii) the modification of the matrix composition by doping (chemical contribution). The damage in UO_2 single crystal irradiated with 470 keV Xe ions was studied by *in situ* RBS/C experiments and two main steps in the disordering kinetics were observed [20]. The first damage step around 0.1 at.% Xe is related to radiation damage, i.e. formation of extended defects, like tangled dislocations. The second damage step around 10 at.% Xe is related to a fracturation of the crystal due to large stress induced by overpressurised gas bubbles. In the present study with similar irradiation conditions, no cracks were found in the whole dose range from 5×10^{14} to 1×10^{16} ion/cm^2 (Xe content at a peak value from around 0.1 at.% to 2 at.%). Thus the ballistic contribution should be the main kinetics of radiation damage.

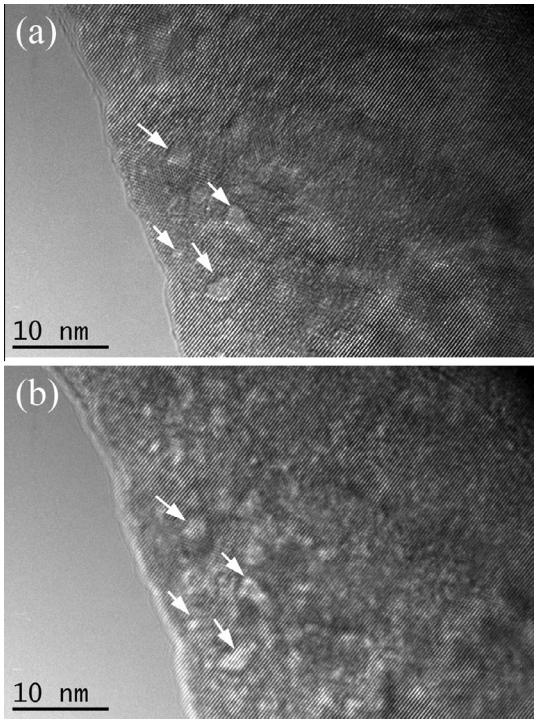

Fig. 5. HRTEM images of bubbles in UO_2 single crystal irradiated with 300 keV Xe at room temperature at a dose of 5×10^{14} ions/cm^2. (b) is an underfocus image of (a). Some bubbles are marked by arrows.

Fig. 6 shows the STEM/EDS/EELS images of 300 keV Xe-irradiated UO_2 single crystal at 1×10^{16} ions/cm^2. Fig. 6(a) shows the typical EDS spectrum at a foil thickness around 50 nm calculated

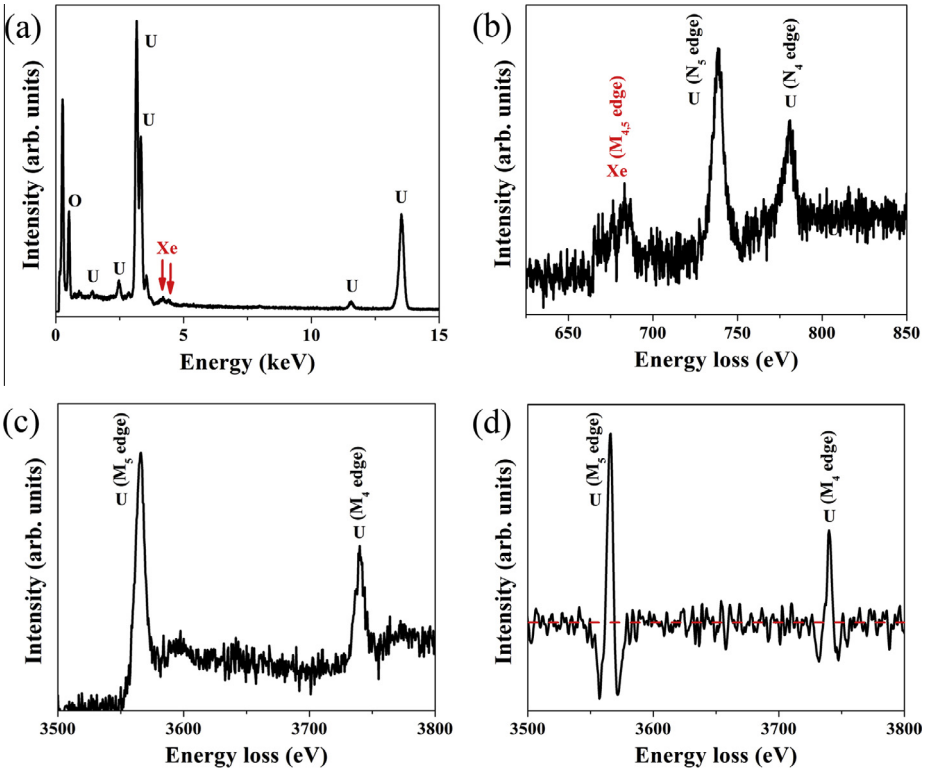

Fig. 6. (a) EDX and (b) and (c) EELS spectra of UO_2 single crystal irradiated with 300 keV Xe at room temperature up to a dose of 1×10^{16} ions/cm^2. (d) The second derivative EELS spectrum of part (c).

by a thickness fringe method [6]. Weak xenon peaks can be identified at the energy range of 4–5 keV. The EDS quantitative analysis was not given here since the Xe content in TEM foil is too low to be measured accurately. The implanted Xe can also be detected by EELS (Fig. 6(b)). The Xe $M_{4,5}$-edge presents at 670 eV, which is lower than the U $N_{4,5}$-edge. To reveal the stoichiometry of irradiated UO_2, the EELS measurement for U M ionization edge was conducted (Fig. 6(c)). The M_4 and M_5 white line edges correspond to the transition of a 3*d* core electron into an excited 5*f* final state. Numerous studies have demonstrated that a change in valence state of rare earth and actinide cations introduced significant changes in the M_5/M_4 white-line ratios [21,22]. To exclude the white line intensity contributions from the background, the second derivative numerical filtering technique was used and the EELS second difference spectrum of $M_{4,5}$-edge is shown in (Fig. 6(d)). Afterwards, the U-M edge intensities were determined by integrating the intensity of the respective peaks above the zero-value linear function (red dashed line in Fig. 6(d)). Colella et al. [23] have established the proportionality between the measured U-M branching ratio and the 5*f* occupancy of U. Following the method by the Colella et al., we calculated the branching ratio of M-edge of 0.695, which is in the range of 0.695–0.720 for U^{4+}, suggesting that the stoichiometry of UO_2 was unaffected by the Xe irradiation.

4. Conclusions

The *in situ* microstructure evolution in Xe irradiated UO_2 single crystal UO_2 was observed by Transmission Electron Microscopy at room temperature. The dislocation evolution in UO_2 single crystal under room-temperature irradiation was shown to occur as nucleation and growth of dislocation loops at low-irradiation doses, and followed by a transformation to extended dislocation segments and networks at high doses. There is no dislocation denuded zone close to the surface due to high irradiation damage near surface and low irradiation temperature. Nanometer-sized Xe bubbles around 1–2 nm were found in UO_2 single crystal subjected to room temperature irradiation. No solid Xe precipitates in bubbles were revealed by the lattice images. The bubble formation under room temperature irradiation implies that Xe bubbles may directly nucleate at the vacancy clusters produced in cascades at room temperature and such a process does not require Xe and U vacancies to be diffusive. The stoichiometry of UO_2 single crystal was stable during room-temperature irradiation as determined by EELS. The investigation of microstructure evolution in Xe-irradiated UO_2 at room temperature can support the modeling effort of fuel microstructure and enable fundamental studies of thermal transport in Xe-containing UO_2.

Acknowledgements

This work was supported as part of the Center for Materials Science of Nuclear Fuel, an Energy Frontier Research Center funded by the U.S. Department of Energy, Office of Science, Office of Basic Energy Sciences. A portion of this research was supported by the U.S. Department of Energy, Office of Nuclear Energy under DOE Idaho Operations Office Contract DE-AC07-051D14517. The *in situ* electron microscopy observation was accomplished at the Electron Microscopy Center for Materials Research at Argonne National Laboratory, a U.S. Department of Energy Office of Science Laboratory operated under Contract No. DE-AC02-06CH11357 by UChicago Argonne, LLC. We thank Peter M. Baldo of Argonne National Lab for his help in performing the irradiations.

References

[1] D.R. Olander, Fundamental aspects of nuclear reactor fuel elements, Technical Information Center, Office of Public Affairs, Energy Research and Development Administration, (1976).
[2] K. Chockalingam, P.C. Millett, M.R. Tonks, J. Nucl. Mater. 430 (2012) 166.

[3] P.C. Millett, M.R. Tonks, J. Nucl. Mater. 412 (2011) 281.
[4] J.H. Evans, J. Nucl. Mater. 188 (1992) 222.
[5] C. Sabathier, L. Vincent, P. Garcia, F. Garrido, G. Carlot, L. Thomé, P. Martin, C. Valot, Nucl. Instrum. Methods B 266 (2008) 3027.
[6] G. Sattonnay, L. Vincent, F. Garrido, L. Thomé, J. Nucl. Mater. 355 (2006) 131.
[7] A. Michel, C. Sabathier, G. Carlot, O. Kaïtasov, S. Bouffard, P. Garcia, C. Valot, Nucl. Instrum. Methods B 272 (2012) 218.
[8] L.F. He, M. Gupta, C.A. Yablinsky, J. Gan, M.A. Kirk, X.M. Bai, J. Pakarinen, T.R. Todd, J. Nucl. Mater. 443 (2013) 71.
[9] J.W.L. Pang, W.J.L. Buyers, A. Chernatynskiy, M.D. Lumsden, B.C. Larson, S.R. Phillpot, Phys. Rev. Lett. 110 (2013) 157401.
[10] J. Spino, P. Peerani, J. Nucl. Mater. 375 (2008) 8.
[11] J.F. Ziegler, U. Littmark, J.P. Biersack, Calculation using the Stopping and Range of Ions in Matter (SRIM) Code. http://www.srim.org/.
[12] J. Soullard, J. Nucl. Mater. 135 (1985) 190.
[13] R. Stoller, M. Tolozko, G. Was, A. Certain, S. Dwaraknath, F.A. Garner, Nucl. Instrum. Methods B 310 (2013) 75.
[14] A.D. Whapham, B.E. Shelden, Phil. Mag. 12 (1965) 1179.
[15] J. Soullard, J. Nucl. Mater. 78 (1978) 125.
[16] G. Martin, P. Garcia, C. Sabathier, L. Van Brutzel, B. Dorado, F. Garrido, S. Maillard, Phys. Lett. A 374 (2010) 3038.
[17] K. Nogita, K. Une, J. Nucl. Mater. 250 (1997) 244.
[18] K. Nogita, K. Une, Nucl. Instrum. Methods B 141 (1998) 481.
[19] L.F. He, C. Yablinsky, M. Gupta, J. Gan, M.A. Kirk, T.R. Allen, Nucl. Technol. 182 (2013) 164.
[20] F. Garrido, L. Vincent, L. Nowicki, G. Sattonnay, L. Thomé, Nucl. Instrum. Methods B 266 (2008) 2842.
[21] J.A. Fortner, E.C. Buck, Appl. Phys. Lett. 68 (1996) 3817.
[22] D.B. Williams, C.B. Carter, Transmission Electron Microscopy—A Textbook for Materials Science, Plenum, New York, 1996.
[23] M. Colella, G.R. Lumpkin, Z. Zhang, E.C. Buck, K.L. Smith, Phys. Chem. Miner. 32 (2005) 52.